The beginning is now and will always be
"Another Train" by Pete Morton

Chapter 1

Introduction

1.1 Historical Background and Overview

As far back as 1934, Baade and Zwicky predicted the existence of dense, compact objects called neutron stars, forming as the result of the supernova explosion of massive stars, and supported only by neutron degeneracy. These objects were not observed until pulsars were discovered by chance in 1967 (Hewish *et al.* 1968), when Jocelyn Bell found a pulsating radio source with an astonishingly regular period.

The first pulsar discovered, PSR B1919+21[1], had a period of 1.337 seconds. This period meant that pulsars could have been associated with white dwarfs, but the detection of the Crab pulsar by Staelin and Reifenstein (1968), with a period of 33 milliseconds, confirmed the identification of pulsars as neutron stars, as they are the only objects capable of rotating at the required frequency. If the pulsations reflected an orbital period, then the 33 millisecond orbit of the Crab pulsar would be very small. Gravitational radiation from the system would then predict a period decrease, while the observed period increases. Radial oscillations of neutron stars cannot explain the long period pulsars, while radial oscillations of white dwarfs cannot explain periods shorter than about a second. In addition, in these cases we expect that the period should be proportional to $\sqrt{\rho}$. The star's density ρ would then have to span many orders of magnitude to explain the observed range of periods. Thus pulsars must be associated with rotating neutron stars. The Crab pulsar is located in the Crab nebula, which is the site of the supernova explosion observed in 1054 AD by Chinese astronomers. Several other pulsars are associated with supernova remnants (cf. Figure 1.1), supporting the theory that pulsars form in supernovae. Interestingly, Pacini (1967) predicted that a rotating magnetized neutron star might be the energy source required to explain the observed radiation from the Crab nebula.

[1] Pulsar names give the location of the object in the sky, and take one of two forms. B$hhmm+dd$ gives the hours and minutes of the right ascension, and degrees of declination, in the B1950.0 coordinate system. J$hhmm+ddmm$ gives the hours and minutes of right ascension, and degrees and arcminutes of declination, in the J2000.0 coordinate system.

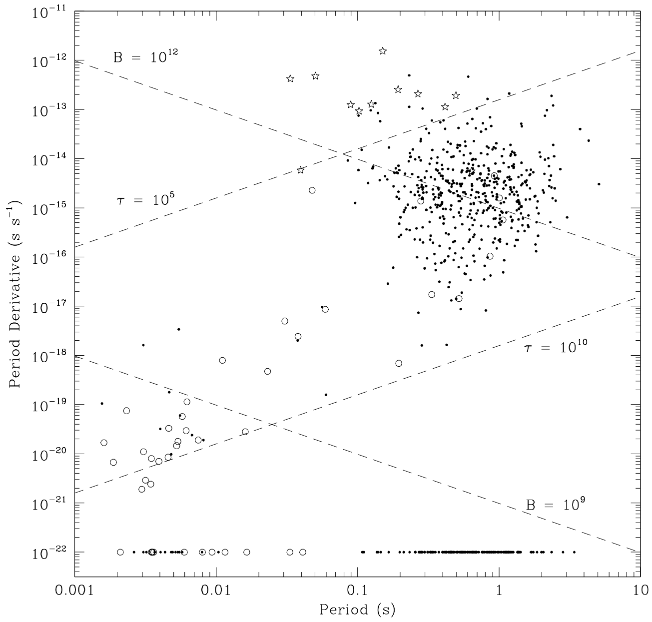

Fig. 1.1.— The observed $P - \dot{P}$ distribution for the pulsars in the current pulsar catalog. Isolated pulsars are designated by single dots, those in binary systems by open circles, and those associated with supernova remnants by stars. Those with $\dot{P} \leq 0$ (either unmeasured, or presumably contaminated by dynamical effects) lie at the bottom of the plot. The dashed lines represent characteristic ages τ of 10^5 and 10^{10} years, and magnetic fields B of 10^{12} and 10^9 Gauss (cf. section 1.5).

A pulsar is therefore a rotating neutron star, which packs 1.4 times the mass of our sun into a sphere only 20 km across and spins once around in less than 5 seconds. One cubic centimeter of its material would weigh about 1 billion metric tonnes on Earth. The radio pulses originate because an emission beam inclined relative to the rotation axis sweeps around like a lighthouse, producing pulses whenever it crosses the line of sight of the observer. In most models, this emission beam is associated with the poles of the strong magnetic field believed to be associated with the neutron star.

More than 700 radio pulsars are currently known with periods from 1.56 ms to 5.09s. All are slowing down due to energy loss. Figure 1.1 displays the period P and period derivative $\dot{P}$ values of the current population. The data were taken from the pulsar catalog publicly available from Princeton (Taylor, *et al.* 1995). Typical "garden variety" pulsars have periods of 100 ms to 2 s (the mean is 0.7 s), and magnetic fields of 10^{12} Gauss (for comparison, the magnetic field of the Earth is of order 1 Gauss). The *spectral index* of the radiation q, is defined by $S_{\nu_1} = S_{\nu_2}(v_1/v_2)^q$, where S_ν is the radio flux. Pulsars have steep radio spectra, with $\bar{q} = -1.6$. As can be seen in Figure 1.1, the period distribution of pulsars is bimodal, and there are two separate populations of pulsars. The Crab pulsar was the fastest pulsar known until the discovery of the population of millisecond pulsars in 1982 (Backer *et al.* 1982). The first such object discovered, PSR B1937+21, has a period of 1.56 ms, and is still the fastest known pulsar. It rotates an astonishing 640 times a second. There are currently about 60 millisecond pulsars known with periods less than $\sim$ 50 ms. The short-period edge of this population is not defined, due to selection effects in pulsar searches. These have typical magnetic fields of $10^8 - 10^9$ Gauss, and are among the oldest pulsars (cf. Figure 1.1). The fraction of millisecond pulsars with binary companions is much larger than that for the slower pulsars. This leads to the theory that they are "recycled" pulsars, spun up due to the accretion of mass from their companions (see reviews in Bhattacharya 1996, van den Heuvel 1995).

Millisecond pulsars are an apparently distinct population, yet their emission properties are in many ways similar to those of their more sedate relatives (the "slow" pulsars). We know surprisingly little about the source of that emission, even 30 years after the discovery of pulsars. The radio emission contains a tiny fraction of the total available spin-down energy. This fact hinders complete understanding of the emission process, which must produce radiation for periods and magnetic fields each spanning 3 orders of magnitude. This is possible because the two classes of objects have similar accelerating voltages B/P^2 (cf. Section 1.5). Despite the similarities, this newer class of pulsars probes new aspects of the radiation emission beam and region. It is hoped that by relating the properties of millisecond pulsars to the models of pulsar emission based on the slower objects, we may improve our understanding of these models. The remainder of this chapter is devoted to summarizing our current knowledge of normal pulsars, then discussing the motivation behind this study of millisecond pulsars.

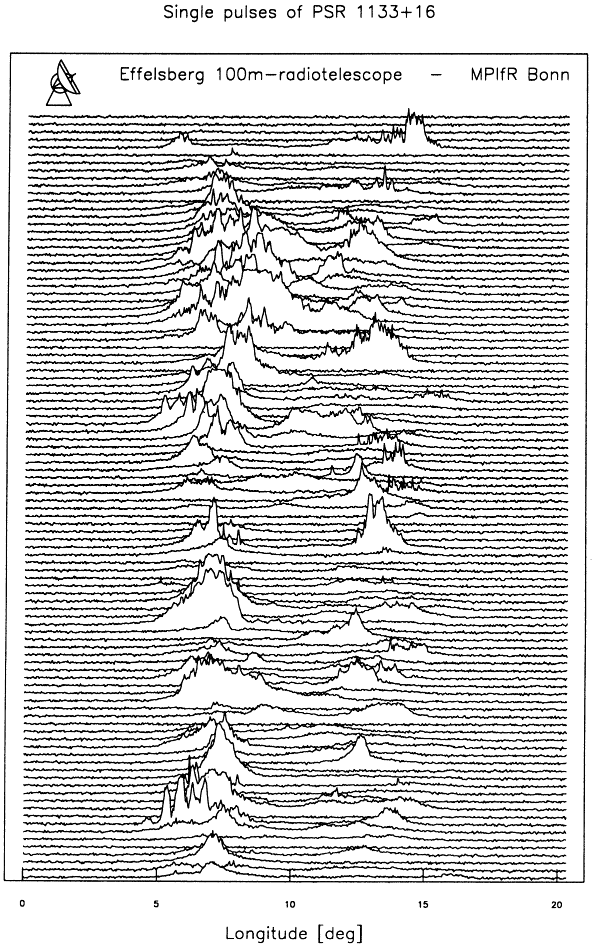

Fig. 1.2.— The measured intensity versus pulse longitude is shown for 100 consecutive single pulses from PSR B1133+16 at 1.41 GHz. One rotation period corresponds to 360° longitude. Both sub-pulses and microstructure are visible. Taken from Kramer (1995).

1.2 Single Pulses

The first pulsar was originally discovered by observations of individual pulses. Studying the single pulses of many pulsars has told us much about pulsar emission. Figure 1.2 displays a sample of individual pulses from the pulsar B1133+16 at 1.41 GHz.

It is customary to plot the intensity of the radiation versus pulse phase, which is usually quoted in degrees of longitude. One rotation of the pulsar corresponds to one pulse period and 360° of longitude. Individual pulses display a large variety in shape, intensity, and exact location within the pulse. Several bursts of emission are often present in a single pulse. These *sub-pulses* are of order 1 ms – 100 ms for typical pulsars. The range of longitudes where emission is observed for a given pulse reflects the location of instantaneous emission within the pulsar magnetosphere. In some pulsars, the location of the sub-pulses drifts systematically from one period to the next (*e.g.,* Backer, Rankin & Campbell 1975). This phenomenon is termed *drifting sub-pulses*.

In addition to the sub-pulses, the single pulse intensities are modulated by *microstructure*, which has a characteristic time scale of 1 μs to several hundred μs for slow pulsars.Both sub-pulses and microstructure are visible in Figure 1.2. Microstructure is sometimes quasiperiodic (*e.g.,* Cordes, Weisberg & Hankins 1990), exhibiting a preferred spacing between micropulses. The phenomenon is broadband, occurring across a wide range of frequencies (Rickett, Hankins & Cordes 1975, Boriakoff & Ferguson 1981), although it does not appear to correlate above and below 1.2 GHz (Boriakoff 1992). The longitude of micropulses does not seem to vary with radio frequency, apart from the dispersive effects due to propagation through the interstellar medium (cf. section 1.8). This contrasts with the sub-pulses whose location in longitude changes with the observing frequency (Boriakoff & Ferguson 1981, Boriakoff 1983), similar to the behaviour of the average pulse profiles (cf. section 1.3).

The pulse intensity changes from one pulse period to the next. One measure of this is the *modulation index*

$$m = \sqrt{\frac{\sigma^2_{E_{on}} - \sigma^2_{E_{off}}}{\bar{E}_{on} - \bar{E}_{off}}}, \tag{1.1}$$

where E_{on} is the pulse energy in the pulse window and E_{off} is the pulse energy at a longitude where there is no pulsed emission. This is 1 for 100% modulation of the time series of pulse energies. In a few pulsars, sometimes the change in intensity from pulse to pulse is extreme. The Crab pulsar was discovered by the detection of its very strong individual pulses, dubbed *giant pulses*. These provide a unique probe of the emission from this pulsar. Until recently, this phenomenon was limited to the Crab pulsar, but the fastest millisecond pulsar, PSR B1937+21, has also been shown to possess giant pulses (Backer 1995, Cognard *et al.* 1996).

The pulsed emission sometimes switches off entirely. This *nulling* behaviour typically lasts from a few pulses to hundreds or thousands of periods. In extreme cases a pulsar may be in the null state well over half of the time (*e.g.,* PSR B0826-34, Durdin *et al.* 1979). Nulling is generally a broadband phenomenon, but does not always occur simultaneously at well separated frequencies (Davies *et al.* 1984, Bartel *et al.* 1982, Bartel *et al.* 1981). Nulling behaviour is correlated primarily with the pulse period (Biggs 1992), indicating that it may be due to a faltering emission mechanism. In pulsars exhibiting both nulling and drifting sub-pulses, the drift rate of the sub-pulses has been seen to change during a null, then relax to the pre-null rate (Lyne & Ashworth 1983). Hence there is some "memory" in the system even while the emission is turned off.

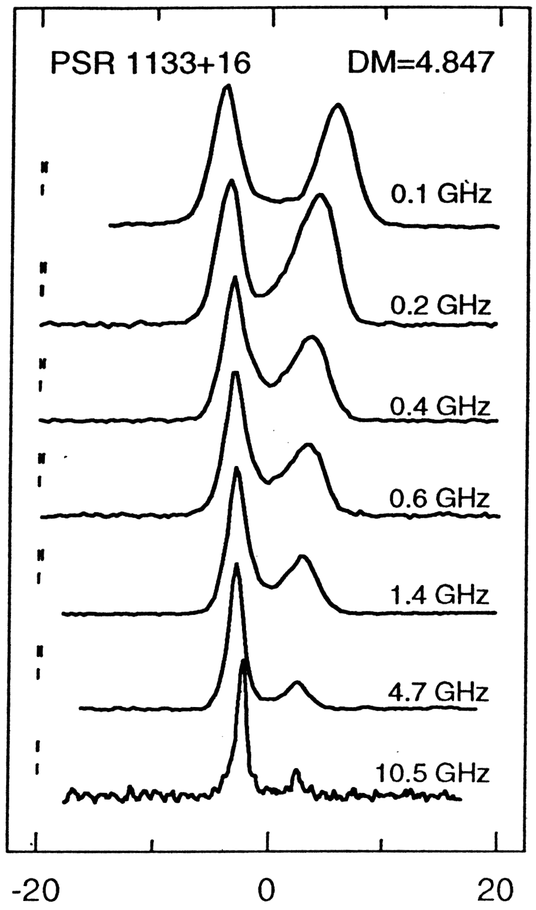

Fig. 1.3.— Average profile of PSR B1133+16 at various radio frequencies. The two components separate with decreasing radio frequency. Taken from Kuzmin *et al.* (1998).

1.3 Properties of Average Profiles: Emission Region

Averaging over hundreds or thousands of pulses leads to an average pulse profile which is remarkably stable for a given pulsar at a given frequency, given the variations in individual pulses. These average profiles stabilize within a few hundred or thousand pulse periods (Helfand, Manchester & Taylor 1975, Rathnasree & Rankin 1995). Figure 1.3 displays the average intensity profile for PSR B1133+16 at several radio frequencies, as a function of pulse longitude. At any given frequency, the average profile has two main components whose longitudes are generally the preferential longitudes of the individual sub-pulses. The average profile is a reflection of the time average of the location of the emission region. The presence of double components in the profiles of many pulsars suggested a *hollow cone* model of emission (Komesaroff 1970). The existence of triple profiles required the addition of a narrow central pencil beam (Backer 1976). This has come to be known as the *core* emission (Rankin 1983a).

The accuracy of pulsar timing depends on the stability of the average profile over long time scales. Since these measurements are made by comparing the arrival of pulses against a standard template of the pulse profile, unidentified changes in the average pulse shape could introduce systematic errors into the results (see Backer 1989, Backer 1996, Kaspi 1995, Taylor 1994, Taylor 1995,Taylor 1996 for pulsar timing reviews). However average profiles are found to be stable over time scales of years. Blaskiewicz (1991) found that only 2 of 14 pulsars showed any profile shape variations over a time scale of 14.5 years. This indicates that the emission beam location remains constant within the pulsar magnetosphere, which itself maintains (on average), a constant configuration. This is undoubtedly due to the presence of the very strong magnetic field. However, some pulsars display an unusual behaviour known as *moding*, in which the pulsar changes its profile by a large amount, into a new stable configuration (eg. Rankin 1986, Bartel *et al.* 1982). This new profile lasts for a few periods to hundreds of periods, then the profile returns to another mode. Moding is a broadband phenomenon, occurring simultaneously in PSR B0329+54 at both 1.4 and 9.0 GHz (Bartel *et al.* 1982). Mode changes usually affect the average profile mainly by varying the intensity ratios of the components, and through small shifts in component separations. The polarization properties are also changed during a mode change. Bartel *et al.* (1982) suggest that the nulling, moding, and drifting-subpulse phenomena may all be related. A comprehensive list of pulsars exhibiting these phenomena may be found in Rankin (1986).

Based on the above observations, the basic pulsar model is believed to be that of a highly magnetized, rapidly rotating neutron star. The dipolar magnetic field is frozen into the crust and corotates with the pulsar out to the distance of the *light cylinder*, r_{LC}, where the speed associated with rotation reaches the speed of light. The light cylinder for a 1 s pulsar is $\sim$ 48000 km. The region in which the magnetic field lines do not close within the light cylinder is called the *open field region*. On the surface of the neutron star, the *polar cap* is defined by the open field lines. The emission beam is assumed to be a hollow cone with a central component, centered on the magnetic dipole axis, and confined to the open field region above the polar cap. A schematic diagram of the pulsar system for a generic polar cap model is shown in Figure 1.4.

Figure 1.5 shows the possible profiles resulting from various lines of sight across the beam, from a point of view above the polar cap. A line of sight grazing the edge of the emission cone results in a single component profile; a line of sight closer to

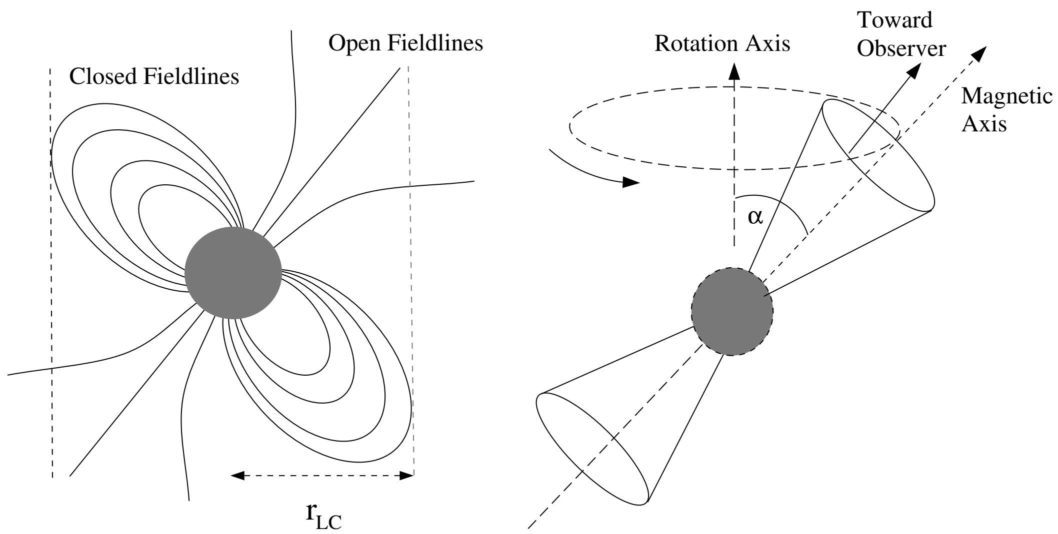

Fig. 1.4.— A schematic diagram of the pulsar configuration. The light cylinder distance r_{LC} is the distance beyond which the corotation velocity would exceed the speed of light. The emission is generated above the polar cap, which is defined on the neutron star surface by the magnetic field lines which do not close within the light cylinder. A hollow cone emission beam is therefore centered on the magnetic axis, which is inclined relative to the rotation axis by an angle α. This sweeps past the observer like a lighthouse beam, resulting in the radio pulse. Adapted from Kramer (1995).

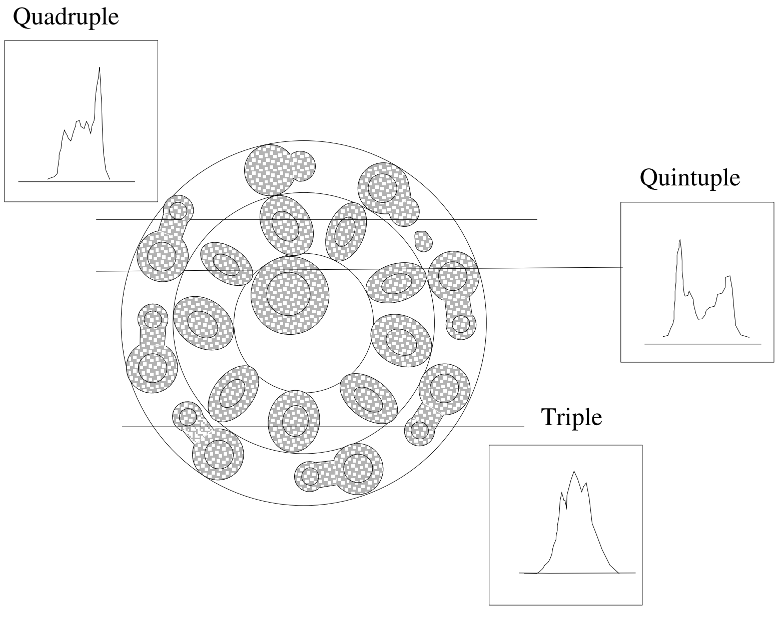

Fig. 1.5.— A schematic diagram showing the possible profiles resulting from various lines of sight across the pulsar beam, which is considered to be a double hollow cone with a central core component. This pulsar beam can result in single, double, triple, quadruple, and quintuple component pulse profiles. Adapted from Rankin (1993a).

the center results in two components, one from each edge of the cone; and a line of sight through the central core results in a triple profile. Rankin introduced a second hollow cone in order to explain pulse profiles with five components (Rankin 1993). The average profiles of some pulsars have two components nearly 180° apart. The weaker *interpulse* is interpreted as emission from the magnetic pole opposite to that of the main pulse, indicating that the *inclination angle* α between the rotation and magnetic axes is nearly orthogonal.

Although the average profile at a particular radio frequency usually remains constant, the shape of the profile changes significantly with frequency. The frequency evolution of the average pulse profiles happens systematically and allows the classification of slow pulsars (Rankin 1983a, 1983b, 1986, 1990, 1993a, 1993b; Lyne & Manchester 1988). Pulse components have been divided into two categories. The central core components already mentioned have steeper spectral indices q than the outer conal components (Rankin 1983a; Lyne & Manchester 1988), frequently have significant circular polarization which changes sign across the pulse profile (see section 1.4; Rankin 1983a), have "white" fluctuation spectra, and do not display drifting sub-pulses (Rankin 1986). Single component pulsars with only core emission exhibit neither moding nor nulling behaviour (Rankin 1986). The *cone* components from the emitting hollow cone have smaller spectral indices, separate with decreasing radio frequency, and occasionally display the drifting sub-pulse phenomenon. Figure 1.3 clearly shows the separation of conal components with decreasing radio frequency.

The quantity $B_{12}/P^2 \propto \left(\dot{P}/P^3\right)^{1/2}$, as will be discussed in section 1.6, measures the acceleration potential available to the particles responsible for the emission. Here the magnetic field is measured in units of 10^{12} Gauss. Pulsars with $B_{12}/P^2 > 2-3$ are dominated by core radiation, while small values of B_{12}/P^2 are associated with pulsars dominated by conal components. Similarly, the parameter $Q = 2P^{1.1}/\dot{P}_{-15}^{-0.4}$ of Beskin, Gurevich, & Istomin (1986, 1988), designed to discriminate between emission modes in their model, separates core and conal pulsars, with $1/Q > 1$ for core emission and $1/Q < 1$ for conal emission, where $\dot{P}$ is measured in units of 10^{-15} s s^{-1}.

The difference in spectral index between the core and cone components means that the core components dominate at low frequencies, while the cone components become more prominent at higher radio frequencies. This difference may be due either to an intrinsic difference in the emission mechanism (Rankin 1990, Rankin 1983a, Weatherall & Eilek 1997) or to purely geometrical effects (Kramer *et al.* 1994, Sieber 1997). It is a function of pulse period, and is greatest for short period pulsars. Most pulsars fit into this classification scheme to explain profile evolution with radio frequency, although there are exceptions (see *e.g.,* Hankins & Rickett 1986).

The observed longitude difference between pulse components can be due to either angular or vertical separation of the emission region for the various components. Pulse components emitted at lower altitudes arrive later than those emitted at higher altitudes, resulting in a difference in the observed pulse longitude. The observed arrival separation of pulse components emitted at the same altitude is due entirely to their horizontal (angular) separation. If the conal components are in fact emitted at a higher altitude, then the core component should be delayed relative to the symmetry center of the conal components. This is seen in many, but not all, triple component profiles.

In the context of the polar cap models with dipolar magnetic fields, Rankin (1990) found that the core components of pulsars of period P with interpulses (which must all be orthogonal rotators with $\alpha \sim 90°$) follow the relation pulse FWHM (full width at half maximum) $\Delta\Phi \sim 2.45° P^{-1/2}$ for slow pulsars at 1 GHz. The angular size of the last open field line has diameter

$$2\rho \approx 2.49° r_6^{1/2}/P^{1/2}, \tag{1.2}$$

where r is the emission radius in units of the neutron star radius, taken to be 10 km. Thus the observed relation is very nearly the angular size of the last open dipolar magnetic field line at the surface of the neutron star. If the radiation completely fills the open field region, then these components must originate very near the surface of the neutron star to explain the observed widths. They may be emitted at a higher altitude if the components do not fill the open field region. For pulsars which are not orthogonal rotators, we expect the apparent width to be scaled by $1/\sin(\alpha)$. If we assume that they obey the same law as the orthogonal rotators, a measurement of the pulse width allows an estimate of the inclination angle α. Applying this method to the core components of triple and quintuple pulsar profiles allows a determination of α for these pulsars. The observed separations of the symmetric components are then observed to fall along inner and outer cones with radius $4.33° P^{-0.52}$ and $5.75° P^{-1/2}$. If they also originate from the last open field line, then they are emitted at altitudes of 130 and 220 km at a radio frequency of 1 GHz. On the other hand, the dependence on pulse period of the conal component *widths* has not been investigated in detail. For short and long-period pulsars, the similar profile morphologies suggest that this quantity scales with the conal component separation, and therefore also scales with $P^{-1/2}$.

The Monte Carlo simulations of Gil & Han (1996) have also indicated that the pulsar beam size is bimodal with a $P^{-1/2}$ dependence. Lyne & Manchester (1988), however, find a somewhat different relation of pulse width on pulse period, with $\Delta\Phi \sim P^{-1/3}$. Biggs (1990) re-analyzed the same data including the effects of non-circular emission beams, and found the results consistent with $\Delta\Phi \sim P^{-1/2}$. Lyne

& Manchester (1988) also argue for a gradual change in emission properties from the inside to outside of the emission region, rather than two distinct types (core and cone) of emission. In their view, all pulse components are emitted at the same height, along different magnetic field lines within the open field region. The various components arise from the patchy nature of emission within this beam. Investigation of the behaviour of sub-pulses by Gil & Krawczyk (1996) provides one argument that the beam is conal, not patchy. In addition, Gil, Kijak & Seiradakis (1993) confirm the hollow cone component distribution found by Rankin, and argue that a flaw in the analysis of Lyne & Manchester (1988) resulted in the evidence for a patchy beam. They argue, however, for a constant altitude of emission. In further support of this view, Gil (1991) conclude on the basis of dual frequency single pulse observations that the core and conal components of PSR B0329+54 originate at same altitude, indicating that the core emission does not fill the open field region.

Pulse profile studies of slow pulsars have concluded that pulsar radiation is generally emitted at a radius corresponding to a few or a few tens of stellar radii, as was found by Rankin above. Timing measurements at two frequencies place a limit on the departures from the interstellar dispersion delay (cf. section 1.8.1), resulting in a limit on the size of the emission region (Cordes 1978, Phillips 1992, Phillips &Wolszczan 1992). Assuming a dipolar field then places an upper limit on the lower edge of the emission region. Cordes & Stinebring (1984) used multifrequency timing measurements of the millisecond pulsar PSR B1937+21 to restrict the range of emission radii to less than 2 km, for radio frequencies 0.3 to 1.4 GHz. More typically, the emission region is limited to a few hundred km, within a few percent of the light cylinder radius. Scintillation studies have resulted in similar estimates (*e.g.,* Cordes, Weisberg & Boriakoff 1983, Smirnova & Shishov 1989), except during episodes of multiple imaging, when the estimates are near the light cylinder (*e.g.,* Wolszczan & Cordes 1987, Kuzmin 1992). Gwinn *et al.* (1997) used scattering / scintillation to limit the size of the emission region of the Vela pulsar to 500 km, as compared to a light cylinder of 4300 km. Finally, the inclusion of relativistic effects on the polarization profile causes an overall time delay by $4R_e/c$ of the symmetry center of the polarization position angle (PPA) profile relative to that of the intensity profile (cf. section 1.4). This method is independent of assumptions about the magnetic field, and yields emission radii of 100 to 1000 km (Blaskiewicz *et al.* 1991). von Hoensbroech & Xilouris (1997) use both profile widths (and the assumption that the radiation comes from the last open field line) and this relativistic effect to conclude that the emission originates at an altitude of $1-2\%$ of the light cylinder radius.

The integrated profiles typically broaden with decreasing radio frequency; single components broaden, while conal components separate. This is often interpreted as a radius to frequency mapping. Lower frequencies are emitted higher in the magnetosphere, where the opening angle of the last open field lines is larger. This explains the general evolution of pulse profiles with frequency in Figure 1.3. More specifically, observers find that the observed widths follow the law $\Delta\Phi = A\nu^{-p} + \Delta\Phi_{min}$, for data ranging from 0.1 GHz to 10 GHz (Thorsett 1991, Xilouris *et al.* 1996). At low frequencies, the widths follow a power law, but at high frequencies, there is little change in width with frequency. Observed values of the power law exponent p vary from pulsar to pulsar, but the averages obtained are $\bar{p} \sim 0.1 - 0.3$ (von Hoensbroech & Xilouris 1997a, Thorsett 1991, Kijak & Gil 1997, Kramer *et al.* 1994, Gil & Kijak 1993, Kramer *et al.* 1997, Rankin 1983b). Theoretically, radius to frequency mapping is expected from any model where narrowband emission occurs at a frequency which varies with distance from the surface of the neutron star. Predictions range from $p = 0.14$ to $p = 2/3$ (*e.g.,* Beskin, Gurevich & Istomin 1988, Ruderman & Sutherland 1975).

An alternative interpretation of the data is that the pulse broadening is due to a propagation effect. Broadband emission originates within a narrow range of radius. At high frequencies, the ray paths are straight, so the beam width is independent of frequency, but at low frequencies, refraction causes pulse broadening. Such behaviour is found in models involving propagation of two modes in a birefringent medium (Barnard & Arons 1986, McKinnon 1997). This model can explain those cases where the core component is ahead of the symmetry center of the conal radiation, and the fact that we do not always observe expected altitude delay effects in timing measurements. In particular, only a 2 km range in radius is implied by timing measurements of PSR B1937+21 (Cordes & Stinebring 1984). This model is also attractive for explaining the polarization behaviour of pulsars (cf. section 1.4). The width of the emission beam is determined in this model by pulse widths at high frequencies. Assuming that the emission follows the last open field line, the emission radii are $\lesssim 100$ km (McKinnon 1997). McKinnon (1997) also notes that the model-independent emission heights derived by Blaskiewicz *et al.* (1991) are consistent with emission at a single radius.

The characteristic shape of the emission beam has been a subject of considerable controversy. Jones (1980) and Narayan & Vivekanand (1983) found evidence for beams elongated along the direction of the local longitude, perpendicular to the trajectory of the line of sight. Lyne & Manchester (1988) found no evidence for elongated pulsar beams, and argued for a circular beam. Using the same data set, Biggs (1990) argued that the pulsar beam is compressed along longitude lines, consistent with the expected geometry of the polar cap region for $\alpha \neq 0$. Gil & Han (1996) used Monte Carlo simulations to conclude that the emission beam is circular or slightly elliptical in this same sense.

1.4 Polarization Properties: Pulsar Geometry

The polarization properties of pulsars have enhanced our understanding of these objects. Single pulse studies (*e.g.,* Manchester, Taylor & Huguenin 1975, Backer, Rankin & Campbell 1976) indicate that the degree of polarization varies strongly from one pulse to the next, from very little to almost 100%. Recently, data at 10.55 GHz indicates that the stronger pulses are more weakly polarized (Xilouris *et al.* 1994), while the evidence at lower frequencies suggests the opposite (Rathnasree & Rankin 1996). The polarization position angle (PPA) change of individual sub-pulses is typically less than 30°, with rapid changes usually attributed to the overlap of two sub-pulses with different position angles (Manchester, Taylor & Huguenin 1975). Boriakoff (1996) notes that subpulses generally follow the polarization angle of the average profile (see below). Cordes & Hankins (1977) found that at 430 MHz the PPA remains approximately constant across micropulses, changing only near the edges. Above 1.7 GHz, the PPA of micropulses in PSR B1133+16 may be as found above, or it may sweep up to 60° (Ferguson & Seiradakis 1978). The polarization properties of micropulses can be vastly different from those of the sub-pulse on which they are superimposed (Boriakoff 1996).

The polarization properties of the average profile can be very different from those of the individual pulses, but are usually stable. According to Rathnasree & Rankin (1995), the stabilization rate of polarization profiles correlates with the opening angle of the last open field lines, ρ. Even if the sub-pulses have a large degree of linear polarization, the superposition of many pulses can have a depolarizing effect on the average if the position angle fluctuates from pulse to pulse. Despite this, average pulse profiles are often highly polarized. Some are nearly 100% linearly polarized while others are not. Some pulsars exhibit no significant circular polarization, while pulsar B1702-19 is 60% circularly polarized (Biggs *et al.* 1988). As mentioned in section 1.3, sense-reversing circular polarization is often associated with core components. The polarization position angle (PPA) of the linearly polarized radiation is usually symmetric and independent of frequency, often displaying either a linear gradient or an S-shaped curve across the pulse. The linear polarization of core components may be disorderly (Rankin 1983a). Figure 1.6 displays the polarization properties of the average profile for pulsar B0355+54 at 1.41 GHz. The first component has a high degree of linear polarization, while the second half of the profile is much less polarized. This profile also has significant circular polarization which changes sense part way through the pulse.

The polarized fraction of pulsars is generally constant up to some frequency, and then decreases with increasing radio frequency (Morris *et al.* 1981, Manchester, Taylor

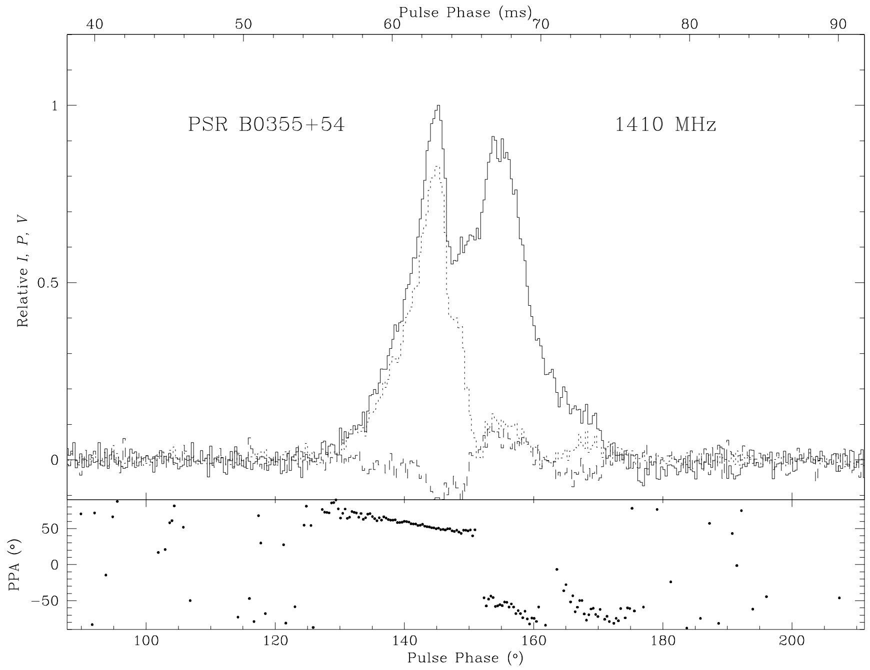

Fig. 1.6.— Polarization profile of pulsar B0355+54 at 1.41 GHz. Solid, dotted, and dot-dashed lines represent the relative intensity, linear, and circular polarizations respectively. The polarization position angle (PPA) is plotted as squares in the lower panel for all points where the linear polarization is greater than the off-pulse rms. The data were taken at the 100-m telescope at Effelsberg with the EBPP (Effelsberg–Berkeley–Pulsar–Processor). The first component is highly linearly polarized, while the remainder of the profile is not. The PPA changes smoothly across the pulse, apart from the abrupt orthogonal mode changes of 90° and associated depolarization. The circular polarization changes sense across the profile, behaviour which is usually associated with a core component.

& Huguenin 1973). In addition, this depolarization appears to correlate with the frequency behaviour of other pulsar parameters, such as pulse width and flux density (Xilouris *et al.* 1996). The depolarization index and the accelerating potential are anti-correlated (Xilouris *et al.* 1995).

Polarization studies led Radhakrishnan and Cooke (1969) to propose a rotating vector model (RVM) which successfully explains the sweep of position angle seen across average pulse profiles of slow pulsars. In this model, the emission which originates near the pole of a dipolar magnetic field is linearly polarized along a direction fixed with respect to the local field. The position angle is then observed to follow the projected direction of the magnetic field. The geometry of the emission region in this model is indicated in Figure 1.7. The inclination of the magnetic axis $\mathbf{B}$ relative to the rotation axis $\mathbf{\Omega}$ is α. The emission beam is centered on $\mathbf{B}$ and has radius ρ. The angle between $\mathbf{B}$ and the observer's line of sight $\mathbf{n}$ attains its minimum value, the

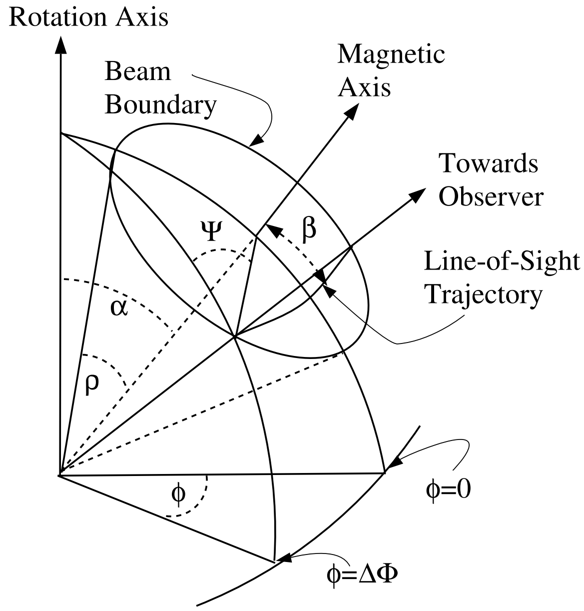

Fig. 1.7.— Geometry of the pulsar emission region as defined by Manchester & Taylor (1977), Rankin (1983a) or Lyne & Manchester(1988). The magnetic axis is inclined relative to the rotation axis by an angle α. The observer's line-of-sight passes through the emission cone with opening angle ρ. The closest approach of the line-of-sight to the magnetic axis occurs at longitude $\phi = 0°$, and defines the impact parameter β. The polarization position angle ψ is measured relative to the projected direction of the magnetic axis. Taken from Kramer (1995).

impact parameter β, when the pulse longitude ϕ is zero. The polarization position angle of the linearly polarized radiation, ψ, is measured with respect to the projected direction of the magnetic axis.

In this formulation, the pulse width $\Delta\Phi$ corresponding to the beam radius ρ is given by

$$\sin^2\left(\frac{\Delta\Phi}{4}\right) = \frac{\sin[(\rho/2)+(\beta/2)]\sin[(\rho/2)-(\beta/2)]}{\sin\alpha\sin(\alpha+\beta)}, \tag{1.3}$$

the position angle follows the relation

$$\tan(\psi) = \frac{\sin\alpha\sin\phi}{\sin(\alpha+\beta)\cos\alpha - \cos(\alpha+\beta)\sin\alpha\cos\phi}, \tag{1.4}$$

and the gradient of position angle reaches its maximum when $\phi = 0°$:

$$\left(\frac{d\psi}{d\phi}\right)_{\max} = \frac{\sin\alpha}{\sin\beta} \tag{1.5}$$

Figure 1.8 displays the rotating vector model sweep for several different geometries. The steepest slopes at longitude $\phi = 0°$ are attained for small values of the impact

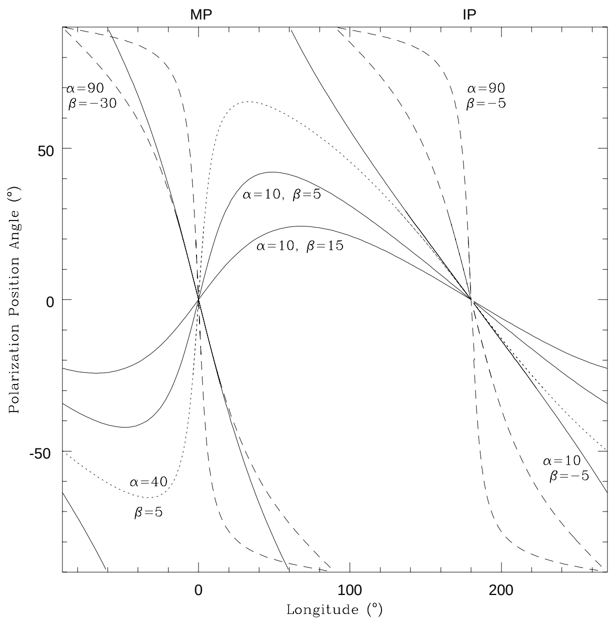

Fig. 1.8.— Rotating vector model of Radhakrishnan & Cooke (1969) for various geometries. Solid lines denote models with magnetic inclination $\alpha = 10°$. Two of the $\alpha = 10°$ models have an impact parameter of $\beta = 5°$, differing only in the sign. This has an enormous impact on the resulting position angle curve. A larger impact angle $\beta = 15$ results in a smaller maximum slope. The effects of different α for different β are seen in the $\alpha = 90°$ (dashed lines) and $\alpha = 40°$ (dotted line) models.

parameter β. The slopes for the main pulse and interpulse are the same for positive β, and opposite for negative β (line of sight between the rotation and magnetic axes). The slopes at the main pulse are nearly the same for $\alpha = 90°, \beta = -30°$ and $\alpha = 10°, \beta = -5°$, but the behaviour at longitudes away from 0° is quite different. The rotating vector model explains the observed sweep of polarization position angle for many pulsars.

Observations of the polarization position angle in principle allow a determination of α and β. The observed pulse width can then be corrected for the effects of the inclination α to provide a value for the beam size ρ. In practice, different values of the inclination angle α mainly affect the wings of the profile, where the data are of poorer quality. The observed central slope provides a relationship between values of α and β via equation 1.5.

Rankin (1990) and Lyne and Manchester (1988) used fits to the polarization angle swing to help determine the geometric angles for many pulsars. Early results indicated that smaller values of the inclination angle α were preferred (Narayan & Vivekanand 1982, Rankin 1990), although Lyne & Manchester (1988) concluded that this was true primarily for older pulsars, with the younger population displaying a more random distribution. McKinnon (1993) corrected Rankin's data for the meridional beam compression noted by Biggs (1990), and found consistency with a random distribution of inclinations, with no evidence for alignment or counteralignment of the magnetic and rotational axes with time. Using Monte Carlo simulations, Gil & Han (1996) also argue that the distribution of observed inclinations ($\sim \sin\alpha$) is matched by a uniform intrinsic distribution of α.

Not all position angle curves follow the rotating vector model. The PPA in Figure 1.6 displays two abrupt discontinuities in an otherwise smooth progression across the pulse. Such unexpected deviations from simple curves have been successfully interpreted through single pulse polarization observations (Backer, Rankin & Campbell 1976, Backer & Rankin 1980, Stinebring *et al.* 1984a, 1984b). The radiation occurs in two polarization modes, with orthogonal position angles. The two competing modes of emission each trace out a position angle curve consistent with the rotating vector model. A 90° jump in the observed angle occurs when a new mode becomes dominant. The superposition of sub-pulses of different PPAs can result in depolarization of the average, which is frequently observed at such an *orthogonal mode* transition. This effect is visible in the profile shown in Figure 1.6. Gil and collaborators (Gil, Snakowski & Stinebring 1991, Gil *et al.* 1992) have carefully separated the polarization modes in several pulsars, and shown that the polarization modes are not always separated by 90°. The deviations from orthogonality are typically 30°, but may be as much as 60°. The dominant mode follows the rotating vector model, but the weaker one does not always do so. There is also evidence that the two orthogonal polarization modes are associated with the core and cone modes of emission (Gil 1986, Rankin 1988, Radhakrishnan & Rankin 1990).

The observations of these orthogonal modes can be explained in terms of two different modes of propagation through the magnetosphere. The emission mechanism must produce radiation in a mixture of the two modes. In the "adiabatic walking" model of Cheng & Ruderman (1979), the polarization directions of the two propagation modes have a different dependence on $\mathbf{B}$, which bends away from the emission cone, resulting in orthogonal PPAs for the two ray bundles. The more intense mode determines the observed polarization state. More generally, one propagation mode propagates along the magnetic field lines, which separates it from the other mode. This splits the beams for the two polarization states, so orthogonal positional angle changes can occur even if the two beams have equal intensities. At some radius, the conditions in the magnetosphere change so that the second mode no longer follows the magnetic field. This radius is frequency dependent, resulting in the mimicking of the effects of a radius to frequency map. At this *polarization limiting radius*, the polarization properties of the emission are finalized. The pulse width and polarization reflect conditions at this radius, rather than at the altitude of emission. Barnard (1986) examines this radius, and finds it to be near the light cylinder, which has a significant impact on the predicted shape of the sweep in position angle. If the initial modes of emission are orthogonally polarized, the separation of these beams can result in a change of the dominant mode with pulse longitude. At high frequencies, the two beams of the two modes are not separated, resulting in depolarization of the profiles due to competition between the modes.

The circular polarization properties of the radiation are difficult to explain. It is almost always associated with the core components of radiation, and the direction of anti-symmetry (when present) of the circular polarization is correlated with the direction of the sweep of the linear polarization position angle (Radhakrishnan & Rankin 1990). Symmetric circular polarization is apparent in other profiles. Many models attribute the circular polarization to the effects of propagation through the magnetosphere (*e.g.,* Cheng & Ruderman 1979, Beskin, Gurevich & Istomin 1988, Kazbegi, Machabeli & Melikidze 1991). Radhakrishnan & Rankin (1990) argue that the correlation with the PPA sweep of the linear polarization, which is determined by purely geometric effects, implies that the anti-symmetric circular polarization is also a geometric property of the emission mechanism. The symmetric circular polarization is again attributed to a propagation effect.

1.5 Basic model

The emission in the basic pulsar model introduced in section 1.3, is powered by magnetic dipole radiation, and the energy loss results in the decrease of rotational energy (Ostriker & Gunn 1969).

For radiation produced in a vacuum, the pulsar slows down at a rate given by

$$-\frac{d}{dt}\left(\frac{1}{2}I\Omega^2\right) = \frac{2}{3c^3}|\mathbf{m}|^2\Omega^4\sin^2\alpha \tag{1.6}$$

where $\Omega = 2\pi/P$ is the angular velocity, I is the moment of inertia, and α is the inclination angle between the magnetic moment, $\mathbf{m}$, and the spin axis. For constant moment of inertia (no loss of mass), the change in angular velocity is governed by

$$\dot{\Omega} = -\left(\frac{2m^2\sin^2\alpha}{3c^3 I}\right)\Omega^3. \tag{1.7}$$

The braking index, n, is defined by

$$\dot{\Omega} \propto \Omega^n, \qquad n = \frac{\ddot{\Omega}\Omega}{\dot{\Omega}^2},$$

and is 3 for magnetic dipole radiation. This has been measured for a few pulsars and is found to be somewhat lower (see Lyne *et al.* 1996 and references therein), which may be caused by the presence of a particle wind, or variations in the moment of inertia, inclination α, or dipole moment. Nonetheless, integrating this equation gives an estimate of the *characteristic age* τ of the pulsar:

$$\tau = \frac{1}{n-1}\left(\frac{\Omega}{\dot{\Omega}} - \frac{\Omega_i}{\dot{\Omega}_i}\right) = \frac{P}{2\dot{P}} \tag{1.8}$$

for n=3 and the assumption that the initial spin period was much smaller than the current value. The measured value of $\dot{P}$ for a typical slow pulsar is of order $10^{-15}\mathrm{ss}^{-1}$, which leads to characteristic ages of a few million years. Millisecond pulsars have smaller periods, but are observed to have smaller period changes as well, $\dot{P} \lesssim 10^{-19}\mathrm{ss}^{-1}$ (Taylor, Manchester & Lyne 1993, Taylor, *et al.* 1995). The characteristic ages are therefore of the order of a billion years. However, it is unclear that the initial spin period was much less than the current period for these objects (Backer 1998). If that is the case, the age estimates must be revised downwards.

Equation 1.7 also allows us to estimate the strength of the magnetic field $\mathbf{B}$. For $B \approx |\mathbf{m}|/r^3$, the magnetic field at the surface of the star ($r = R_*$) is

$$B_s^2 = \frac{3c^3}{8\pi^2}\frac{I}{R_*^6\sin^2\alpha}P\dot{P}, \tag{1.9}$$

which reduces to

$$B_s = 3.2 \cdot 10^{19} \sqrt{P\dot{P}} \text{ Gauss} \tag{1.10}$$

if we take the moment of inertia to be $I = 10^{45}$g cm^{-3}, the radius of the neutron star to be $R_* = 10$ km, and $\alpha = 90°$. This last assumption of an orthogonal geometry means that equation 1.10 represents a lower limit to the magnetic field. Once again a braking index of $n = 3$ has been assumed, for magnetic dipole radiation. As noted earlier, this leads to typical surface magnetic fields of 10^{12} Gauss for slow pulsars, and 10^9 Gauss for millisecond pulsars (cf. Figure 1.1).

The total energy lost by the pulsar is determined by the rate at which it is slowing down:

$$\dot{E} = -I\Omega\dot{\Omega} = 4\pi^2 I\dot{P}P^{-3}. \tag{1.11}$$

Observed values range from 10^{40} ergs/s to 10^{38} ergs/s. Radio luminosities are typically of order 10^{28} ergs/s, indicating that only a small fraction of the spin-down energy is radiated as radio waves. The *brightness temperature* T_B is defined as the temperature that would be required if the observed radiation were due to blackbody radiation, in the Rayleigh-Jeans approximation:

$$T_B = \frac{c^2}{2k\nu^2}$$

For pulsars, the observed flux F is related to intensity I by $F = \int I \, d\Omega$. An effective solid angle $\Omega_{eff} = (c\Delta t/D)^2$ is used to determine I for the brightness temperature calculation: $I = F/\Omega_{eff}$, where D is the distance to the pulsar, and Δt is the time scale of the observed radiation (the pulse width, for example). Brightness temperatures are typically $\sim 10^{25} - 10^{30}$ K for pulsars.

Pulsars are steep spectrum objects, weakening at high frequencies as noted earlier. At about 100 MHz, the spectrum turns over, while at high frequencies there is a break, and subsequent steepening of the power law(Malofeev *et al.* 1994). At *very* high frequencies there is evidence for a turn-up in the spectrum of some pulsars (Kramer *et al.* 1996).

1.6 Pulsar Magnetospheres

In section 1.5 we restricted our attention to a vacuum magnetic field. Goldreich & Julian (1969) showed, however, that the pulsar must be surrounded by a magnetosphere which substantially exceeds this density. In the case of an aligned rotator, the rotating magnetic field induces in the interior of the star (assumed to be a conductor) an electric field which satisfies

$$\mathbf{E} + \left(\frac{\mathbf{\Omega} \times \mathbf{r}}{c}\right) \times \mathbf{B} = 0.$$

This electric field generates a considerable surface charge density, which then generates an exterior electric field with a non-zero component parallel to the magnetic field at the surface. At the surface of the neutron star, the force due to this electric field will overcome the effects of gravity and atomic binding to strip both electrons and ions from the surface (*e.g.,* Jones 1986, Neuhauser *et al.* 1987, Kossl *et al.* 1988). The pulsar must then be surrounded by a plasma with sufficient charge density to short out the parallel component of this electric field. This Goldreich-Julian density is

$$\rho_{G-J} = \frac{\nabla \cdot \mathbf{E}}{4\pi} = \frac{\mathbf{\Omega} \cdot \mathbf{B}}{2\pi c} \frac{1}{(1 - \left(\frac{\Omega r}{c}\right)^2 \sin^2 \theta\Big)}$$

In the Goldreich-Julian magnetosphere, particles in the closed field region are trapped and corotate with the neutron star. Charges found along the open magnetic field lines leave the system and are constantly replenished from the surface.

The spin-down torque of this aligned rotator model is similar in magnitude to that of magnetic dipole radiation from an orthogonal rotator. Arons (1992) noted that this is essentially a measure of the Poynting flux crossing the surface at the light cylinder.

Certain perturbations in this charge-density structure magnetosphere are unstable, and allow for the possibility of evacuated regions within the Goldreich-Julian magnetosphere (Holloway 1973). All modern pulsar models rely on the presence of such gaps in the magnetosphere.

Ruderman & Sutherland (1975) expected that positive ions would not flow freely from the surface. Thus in a model with the magnetic axis anti-parallel to the rotation axis, the ions necessary to shield out the parallel electric field are not available, resulting in a gap near the surface above the polar cap. This gap sustains a potential difference given by the voltage difference between the magnetic pole and the surface position of the last open field line:

$$\Delta\Phi = \frac{\Omega^2 m}{2c^2} \propto \frac{B}{P^2}, \tag{1.12}$$

and this accelerates the particles to energies up to

$$E = \frac{\Delta\Phi}{2} = 3 \times 10^{12} \frac{R_6^3 B_{12}}{P^2} \text{ eV}. \tag{1.13}$$

Particles within the gap will therefore be accelerated to ultra-relativistic energies. The positrons are accelerated outward along the curved magnetic field lines, and emit curvature radiation with energy

$$E_{photon} = \frac{3}{2}\frac{\gamma^3 \hbar c}{\rho_c} \tag{1.14}$$

where $\gamma = (1 - v^2/c^2)^{-1/2}$. In the presence of a sufficiently strong component of the magnetic field ($B_{crit} \sim 10^{13}$ G) transverse to its motion, photons with energy exceeding twice the rest mass of an electron can decay into an electron-positron pair. Any such pair produced within the gap is immediately accelerated, leading to more high energy photons and the further generation of pairs. The initial, or primary, particles produce a cascade of secondary particles within the gap (Sturrock 1971), which discharges the gap. These primary particles may arise as a result of the electron-positron decay of a stray background gamma photon. The curvature radiation from these primary and secondary beams of particles provides the observed radiation. The system reaches a quasi-stable state for a certain gap thickness.

This type of polar cap model is believed to produce the observed radio radiation, although as noted above it is now believed that ions will also flow freely from the surface.

This problem is overcome in the slot-gap model of Arons & Scharlemann (Scharlemann, Arons & Fawley 1978, Arons & Scharlemann 1979). Due to curvature of the magnetic field lines, the charge density cannot both maintain the Goldreich-Julian value and flow in such a way as to conserve the current. This inconsistency creates an electric potential to accelerate the particles. An alternative acceleration mechanism due entirely to relativistic effects is proposed (Muslimov & Tsygan 1990, 1992). Such effects will certainly influence the calculations of other models.

Polar cap models generally have the difficulty that the star will become charged, due to the current induced by the flow of charges. This can be resolved by a return current, although it is unclear exactly how this will be achieved.

Polar cap models typically require a radius of curvature much smaller than that for a dipole magnetic field in order to produce the observed radiation. Additional multipoles near the surface are postulated in order to solve this problem. However, higher order multipoles are ruled out on the basis of the location of the spin-up line of millisecond pulsars, as they are derived from magnetic torques (Arons 1993).[2] Additionally, Kramer *et al.* (1997) find no evidence for non-dipolar effects.

The frame-dragging effects of general relativity (Beskin 1990, Muslimov & Tsygan 1990, Muslimov & Tsygan 1992) significantly alters the electric potential which accelerates the particles, resulting in much higher energy gamma rays. This effect, combined with an offset dipole, provides agreement between theory and the location of the pulsar "death valley" - the voltage ($\propto B/P^2$) below which pulsars are not seen (Arons 1997).

The surface defined by $\mathbf{\Omega}\cdot\mathbf{B} = 0$ separates the space charges of different sign. This surface is problematic in the standard polar cap model, since some open field lines cross this null surface. Outflowing charges must therefore cross regions of opposite sign. Some models (*e.g.,* Michel 1982, Krause-Polstorff & Michel 1985) limit the plasma-filled zones to polar and equatorial regions, leaving this area empty. In other models, these regions are the source of the acceleration potential, due to the formation of *outer gaps* (Cheng, Ho & Ruderman 1986).

The gamma and X-ray radiation may also come from the polar cap region (*e.g.,* Daugherty & Harding 1982). However, the observed properties of the Crab and Vela pulsars are better described by the outer gap model of Cheng, Ho, & Ruderman (1986) mentioned above. Recently, Romani & Yadigaroglu (1995) investigated in detail the geometry of such a system, and find that it explains many facets of the gamma-ray observations, and the relative longitudes of the gamma and radio emission.

1.7 Pulsar Emission

Any proposed mechanism of pulsar radio emission must be coherent in order to explain the high brightness temperatures of the observed radiation. It must also explain the sub-pulse and micropulse fluctuations, and the polarization properties of the individual pulses. The existence of millisecond pulsars implies that the emission mechanism must work over a broad range in both pulse periods and magnetic fields. Any mechanism which depends strongly on either quantity is unlikely to succeed. The voltage B/P^2 is, however, similar for the two classes of objects.

[2] Millisecond pulsars are spun-up to some limiting period during their evolution. The equilibrium period resulting from accretion at the Eddington rate (radiation pressure balances the gravitational force) depends on the magnetic field of the neutron star, resulting in a relation between P and $\dot{P}$. The spin-up line is simply this relation.

There are three main possible types of pulsar emission mechanisms as outlined by Melrose (1992, 1996). These are (i) coherent emission by bunches, (ii) relativistic plasma emission and (iii) maser emission. In the first of these, a bunch of N charged particles within a volume smaller than $\sim \lambda^3$ (so that coherence is maintained within the bunch) flows along the curved magnetic field lines, emitting curvature radiation as though it were a single macroparticle. Then the power emitted by the bunch is equivalent to N^2 times the power emitted by a single particle in the bunch. This was one of the first mechanisms proposed (cf. Sturrock 1971, Ruderman & Sutherland 1975) and was studied in detail by Buchauer & Benford (1976, 1977). The bunching is due to some instability such as the two-stream instability which results when the primary beam of particles interacts with the much less energetic secondary beam. This emission mechanism is still discussed in the literature (*e.g.,* Gil & Snakowski 1990a, Gil & Snakowski 1990b), especially by observers. Melrose points out, however, that the bunch must take the form of a flat pancake that rotates to keep its normal nearly parallel to the magnetic field, which is a rather unlikely configuration. In addition, proposed instabilities grow too slowly to produce or even maintain the required bunches (Melrose 1992), which lose coherence quickly.

Relativistic plasma emission models produce radiation indirectly. A plasma instability such as the streaming instability discussed above generates turbulence. The energy in the turbulence cannot escape directly, but must be converted by some nonlinear process into escaping waves. In the models among this class there are variations in both the type of plasma instability and the conversion process used to convert the energy into radiation (Asséo 1993, Beskin, Gurevich & Istomin 1986, 1988, Kazbegi *et al.* 1991, Weatherall 1997). The frequency of the resulting emission is determined by the local plasma frequency $\omega_p \propto \sqrt{\Omega B}$ and the Lorentz factor, γ, of the particles that drive the instability (Melrose 1996).

Maser emission in atoms or molecules occurs for an inverted energy population, in which the higher energy level is overpopulated with respect to the lower level. Maser emission mechanisms proposed for pulsar emission require some analog to the inverted energy population. This can occur in a variety of models of curvature drift (Luo & Melrose 1992) or the distortion of magnetic field lines (Luo & Melrose 1995), which are sensitive to the value of the magnetic field B, making it difficult to explain both millisecond and normal pulsars. Another possibility is free electron maser emission (Melrose 1978, Rowe 1995), due to a time-varying component of the electric field parallel to B. In both cases, the emission is produced at some characteristic frequency (see Melrose 1996 for details). Like emission from bunches, maser emission can escape the magnetosphere directly, unlike relativistic plasma emission models.

1.8 Propagation Effects

1.8.1 Dispersion delay in cold plasma

Electrons in a plasma are moved by incident electromagnetic waves. This motion in turn influences the propagation of the wave. As a result, pulses emitted simultaneously at two frequencies will reach the observer at different times.

The plasma frequency ω_p is:

$$\omega_p = \sqrt{\frac{4\pi n_e e^2}{m_e}},$$

where e, m_e and n_e are the charge, mass, and number density of electrons. The cyclotron frequency ω_c is the gyration frequency of an electron about a magnetic field B_0

$$\omega_c = \frac{eB_0}{m_e c}.$$

The wave number k of the radiation is then

$$k_{\mathrm{R,L}} = \frac{\omega}{c}\sqrt{1 - \frac{\omega_p^2}{\omega(\omega \pm \omega_c)}},$$

resulting in a group velocity v_g

$$v_g = \frac{d\omega}{dk} = c\sqrt{1 - \frac{\omega_p^2}{\omega^2}}$$

in the absence of a magnetic field. The resulting delay due to the dispersive medium is then (for $\omega \gg \omega_p$)

$$t_p = \int_0^D \frac{ds}{v_g} = t_0 + \frac{2\pi e^2}{m_e c\,\omega^2}\int_0^D n_e(s)\,ds, \tag{1.15}$$

The difference in arrival time between two frequencies ν_1 and ν_2 is

$$\begin{aligned} \Delta t_{DM} &= \frac{e^2}{2\pi m_e c}\left(\frac{1}{\nu_1^2} - \frac{1}{\nu_2^2}\right)\int_0^D n_e(s)\,ds \\ &= \frac{DM}{2.41033 \cdot 10^{-16}}\left(\frac{1}{\nu_1^2} - \frac{1}{\nu_2^2}\right) \end{aligned} \tag{1.16}$$

where we have defined *Dispersion Measure*, DM, to be the column density in units of cm^{-3} pc and the frequency is measured in MHz. Pulsar observers usually round the dispersion coefficient to $2.410 \cdot 10^{-16}$.

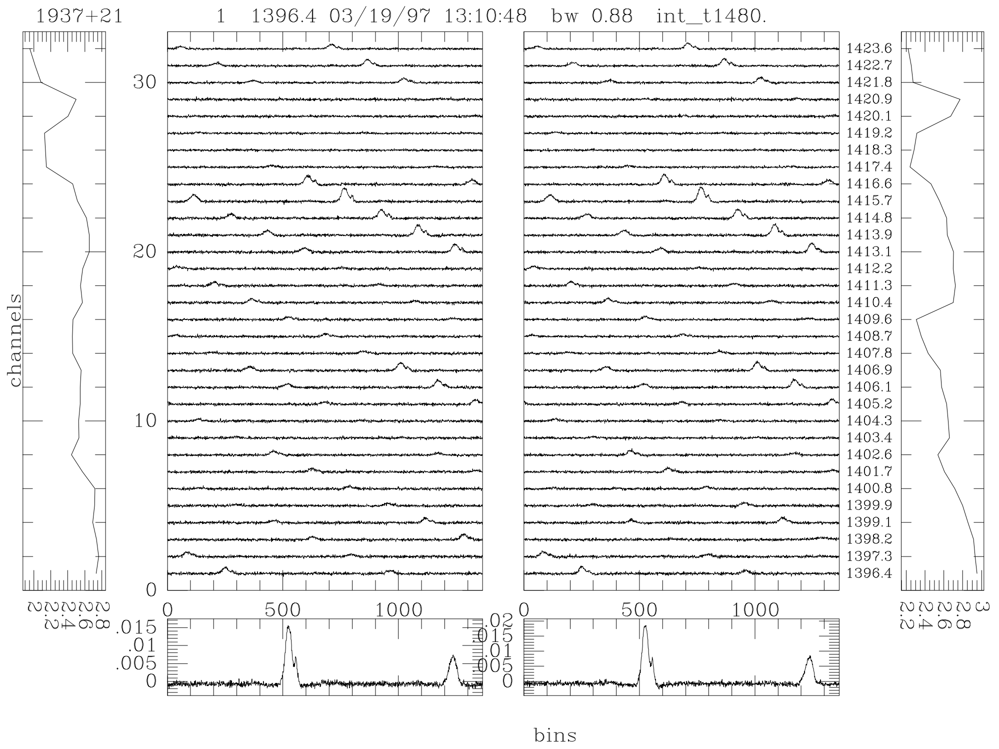

Fig. 1.9.— The differing delay in arrival times due to the dispersion of the interstellar medium for pulsar B1937+21 at 1.41 GHz. The data were taken at the 100-m telescope at Effelsberg with the EBPP (Effelsberg–Berkeley–Pulsar–Processor), which removes the dispersion within each 0.875-MHz channel. The horizontal axis for the central panels is in bins, and covers the full 1.56 ms period of this pulsar. The two large panels display the raw data for left and right circular polarizations, which clearly shows the remaining dispersion delay between channels. In the lower two panels this delay has been removed and the channels have been summed.

The results of dispersion delay are shown for the pulsar B1937+21 at 1.41 GHz in Figure 1.9. The dispersion measure of this pulsar is 71. These data were taken with the EBPP (cf. section 2.2.2), which removes the effects of dispersion within each channel, leaving the delay between channels.

Dispersion Measures vary with time (Backer *et al.* 1993) due to irregularities in the ISM and the relative motions of pulsar and observer.

1.8.2 Faraday rotation

In the presence of magnetic field, the group velocity v_g is different for the two senses of circular polarization. The phase offset between the two circular polarizations increases with distance travelled through the plasma. This introduces a rotation $\Delta\psi$ in the polarization position angle as the radiation propagates through the ionized medium:

$$\Delta\psi = \frac{1}{2}\int_0^D (k_R - k_L)\, ds = \frac{2\pi e^3}{m_e^2 c^2 \omega^2}\int_0^D n_e B_{||}\, ds \qquad \text{radians}, \tag{1.17}$$

where $B_{||}$ is the component of the magnetic field parallel to the propagation path ds, and we have assumed $\omega \gg \omega_p$, $\omega \gg \omega_c$. The *Rotation Measure RM* is then defined as

$$RM = \frac{\Delta\psi}{\lambda^2} = \frac{e^3}{2\pi m_e^2 c^4}\int_0^D n_e B_{||}\, ds = 8.1 \cdot 10^5 \int_0^D B_{||} n_e\, ds \qquad \mathrm{rad\, m^{-2}} \tag{1.18}$$

where $B_{||}$ is measured in Gauss, n_e in cm^{-3}, and distance D in parsecs.

The measured polarization position angle will therefore change with radio frequency, resulting in depolarization of the profile if its effects are not removed across the observing band.

1.8.3 Scattering

The interstellar medium also scatters pulsar signals. In the thin screen approximation, an electromagnetic plane wave is incident on a screen made up of electron-density irregularities, which disturb the phase of the incoming wave. The radiation of wavelength λ is scattered into a cone of width $\Theta_s = \lambda/l_\phi$, where l_ϕ is the transverse length scale over which the phase is perturbed by one radian. The delay due to the extra distance travelled along various paths broadens the pulse. The distribution of scattered radiation is assumed to be Gaussian in angle. As a result, the pulse is broadened by convolution with the impulse response of the thin-screen ISM, which is

$$e^{-t/\tau_B}; \qquad \tau_B = x(1-x)\Theta_s^2 D/c, \tag{1.19}$$

for a thin screen at distance xD and pulsar at distance D. This effect is largest for pulsars with large dispersion measures, where the signal has passed through a large column density of electrons, and is strongly dependent on frequency, becoming more important for long wavelengths.

In addition to pulse broadening, interstellar scattering causes temporal variations in the brightness of a pulsar, known as *scintillation*. The phases of the electromagnetic waves are disrupted during their multi-path propagation through the non-uniform interstellar medium. A pattern of constructive and destructive interference is therefore created. Diffraction occurs when the phase in a wavefront is perturbed by large values within the Fresnel-zone radius. Due to the relative motions in the system, the observer moves relative to this pattern, resulting in time-variations of the pulsar intensity. The intensity variations will occur at different times for different radio frequencies. Such interstellar scintillation variations in the intensity of PSR B1937+21 are visible in the various channels of Figure 1.9.

Large scale gradients and irregularities in the interstellar medium result in refractive scintillation. The irregularities act as weak lenses along the line of sight, distorting the source's intensity by $\sim 25\%$ and possibly its apparent position.

The intensity variations due to interstellar scintillation mean that not all observations of pulsars will result in the same signal-to-noise. The intensity amplification can be extreme in the transition region between strong and weak scattering, if a diffractive maximum occurs within a refractive maximum. Observations taken at times of scintillation maxima are clearly preferred!

1.9 Millisecond Pulsars

Despite their faster spin periods and smaller magnetic fields, the average profiles of millisecond pulsars exhibit many of the same characteristics as those of slow pulsars. Their spectra are the same, although they are slightly less luminous and less efficient (Kramer *et al.* 1998). Their properties do not, however, easily find an interpretation in the well established classification schemes developed by the systematic studies of normal pulsars discussed in section 1.3.

Millisecond pulsars could not be easily studied in detail until recently, due to the increased time resolution required and the difficulty in overcoming the effects of dispersion due to the interstellar medium. The amount of polarization and profile data is increasing, although it is still somewhat limited. Thorsett and Stinebring (Thorsett & Stinebring 1990) obtained polarization measurements at Arecibo for three millisecond pulsars, but only obtained multifrequency polarimetry for one of the objects. Segelstein *et al.* (1986) obtained polarimetry on a single object at a single frequency. Recently, Kramer *et al.* (1997b) and Xilouris *et al.* (1998) reported the results from profile and polarization monitoring of 23 millisecond pulsars at 21cm. There is, however, still a relative paucity of published profiles at other frequencies, and the resolution of the published profiles is sometimes poor.

Such preliminary investigations have shown that decoding the emission geometry of millisecond pulsars will not be simple. The profiles of millisecond pulsars have, on average, one more component than slow pulsars, and are much more likely to have pre- or post-cursors or interpulses (Kramer *et al.* 1998, Ruderman 1991a). Millisecond pulse profiles also have larger duty cycles. The width-Period relation for conal components in slow pulsars scales to a beam width of 180°, and therefore a duty cycle of 1 for a period of 1-4 ms (Kramer *et al.* 1998). This partially explains the large duty cycles, but the widths of millisecond pulsars therefore imply a beam angle narrower than that implied by the scaling law. Similarly, the Rankin core component width-period relation implies a very open magnetic field, and wide pulses for millisecond pulsars. However, Backer (1995) noted that there seem to be unusually narrow components in many millisecond pulsars. As an example, PSR B1937+21 is expected, based on the acceleration potential B/P^2 to be dominated by core emission. Then the predicted pulse width is $\Delta\Phi = 2.45^{\circ} P^{-1/2} = 63^{\circ}$, while the observed width is closer to 10°.

The magnetic field topology in the magnetospheres of millisecond pulsars is a subject of substantial theoretical interest and controversy. A 3 millisecond pulsar has a light cylinder of only 6-10 stellar radii, so the emission (or polarization limiting radius) may occur much closer to the light cylinder. This is supported by emission altitude estimates of Kramer *et al.* (1998). The relativistic delay of the PPA, relative to the symmetry center of the pulse, is a fraction $2R_e/\pi r_{LC}$ of the pulse period, and is therefore most significant for emission close to the light cylinder. Deviations from a dipole magnetic geometry are also expected to affect the polarization position angle data, since the standard rotating vector model is tied to the magnetic field. The expected openness of the magnetic field configuration at large radii leads to the possibility of observing effects due to magnetic field sweepback. The calculations of Barnard (1986) suggest a flattening of the PPA slope for emission (or cessation of propagation effects) near the light cylinder. In addition, the symmetry center of the PPA profile is moved *earlier* relative to the intensity profile, in opposition to the effects of relativistic delay. On the other hand, Gangadhara (1996) finds that even for emission near the light cylinder, the PPA curve will be similar to that for emission near the magnetic pole. In this context, it has been suggested that many pulse-interpulse pairs are actually produced from a single pole, despite their separation by 180° (Gangadhara 1996, Manchester 1996).

Some magnetospheric models anticipate unusual magnetic field configurations for millisecond pulsars, due to the recycling which occurs during their evolution (Ruderman 1991a, 1991b; Chen & Ruderman 1993a). It is possible that these will affect the polarization observations of these objects. The effects of evolutionary behaviour are already evident, since isolated millisecond pulsars have lower luminosity than those in binary systems (Bailes *et al.* 1997, Kramer *et al.* 1998). The evolution of millisecond profiles with radio frequency is larger for less massive companions, resulting in a dependence on pulse period, which depends on the evolution of the system (Kramer *et al.* 1998). Additionally, the spectral indices of millisecond pulsars are correlated with either age or period (Lorimer *et al.* 1995b; Kramer *et al.* 1998).

Polarization measurements are especially interesting for millisecond pulsars in binaries for which we can measure the Shapiro delay. In these systems, the pulses are delayed by the effects of general relativity as the radiation passes the companion, and the measurement of this effect allows the determination of the orbital inclination. If the pulsar spin axis is aligned with the orbital angular momentum vector (a modest assumption), then we know some of the angles in the radio emission system already. Thus polarization observations which help identify the geometry of the emission region for millisecond pulsars are very important.

Thorsett and Stinebring (1990) stress that although the integrated profiles of the pulsars in their small sample exhibit polarization features similar to those seen in slower pulsars, at least two of them do not fit into classifications designed to accommodate slower pulsars. Navarro and Manchester (1996) have studied the polarization of pulsar J0437−4715, and find a very large number of components, with odd variations in position angle. In addition, there is mounting evidence for variation in the pulse profiles and polarization properties of millisecond pulsars (Xilouris *et al.* 1998, Sallmen *et al.* 1997). An unusual example of mode changing is the millisecond pulsar PSR B1821−24, whose second component varies relative to the others on the timescale of days (Backer & Sallmen 1997), which is much longer than the typical moding time scale of slow pulsars. The profiles of several millisecond pulsars also show remarkable development with frequency, containing components with relatively flat spectra (*e.g.,* Fruchter *et al.* 1990; Backer 1995). However, on average the millisecond pulsar average profiles seem to evolve less than the slow pulsars (Kramer *et al.* 1998). In the sample of 1400 MHz polarization profiles (Xilouris *et al.* 1998), the development of the pulse profile with frequency is classified as normal for 4 pulsars, abnormal for 8 pulsars, and 15 pulsars show minimal profile evolution with frequency. If the magnetic fields of millisecond pulsars were greatly disturbed from a dipole, then a radius to frequency mapping would imply a *greater* evolution of profile with frequency, due to the increased dependence of the magnetic field on radius. On average, this is not seen.

Results at single frequencies for the slightly longer period pulsars B1534+12 (Arzoumanian *et al.* 1996) and B1913+16 (Cordes, Wasserman & Blaskiewicz 1990) are not entirely consistent with models developed for slower pulsars, but do possess overall similarities to results for slow pulsars. Thus the pulsars in this transition region may provide a link between the fastest millisecond pulsars and the slow pulsars.

It is clear that polarimetric and multifrequency observations of millisecond pulsars are leading to results which are not simply extensions of the theory developed for slow pulsars. Consistent polarization and profile data at several frequencies are essential to obtain an understanding of these objects.